Journal of Sound and Vibration (2003) **259**(1), 81–96
doi:10.1006/jsvi.2002.5182, available online at http://www.idealibrary.com on IDEAL®

MODAL CHARACTERISTIC OF A ROTATING RECTANGULAR CANTILEVER PLATE

H. H. Yoo

School of Mechanical Engineering, Hanyang University, Sungdong-Gu Haengdang-Dong 17, *Seoul 133-791, Republic of Korea. E-mail: hhyoo@hanyang.ac.kr*

AND

C. Pierre

Department of Mechanical Engineering and Applied Mechanics, University of Michigan, Ann Arbor, MI 48109-2125, *U.S.A.*

(*Received* 17 *May* 2001, *and in final form* 2 *January* 2002)

Modal characteristics of a rotating cantilever plate are investigated in the present work. A dynamic modelling method for rectangular plates undergoing prescribed overall motion is employed to derive the equations of motion. The general equations are particularized for the modal analysis of a rotating cantilever plate and dimensionless parameters are identified through dimensional analysis. The effects of the dimensionless parameters on the modal characteristics of the rotating plate are investigated. Incidentally, eigenvalue loci veering and crossing phenomena along with the corresponding modeshape variations are exhibited and discussed.

1. INTRODUCTION

It is well known that the modal characteristics of flexible structures often change significantly when the structures undergo overall motions. Radial rotating motion of a cantilever beam, for instance, induces centrifugal inertia force which results in the stretching of the structure and effectively increases its bending stiffness. Such phenomena, often referred to as motion-induced stiffness variation effects, have been studied by several researchers due to their practical importance in engineering. Examples of flexible structures which undergo overall motions include rotating blades of helicopters, turbines, and turbo-machines, and flexible spacecraft structures such as satellite antennae and solar energy panels.

Rotating flexible structures have been often idealized as rotating beams since such idealization has provided accurate dynamic characteristics for most rotating flexible structures. Investigations on the vibration of rotating beams have been performed since 1920s. An analytical method to calculate the natural frequencies of a rotating beam was presented by Southwell and Gough [1]. They suggested an explicit equation that relates the natural frequency to the rotating frequency of a beam. This equation, which is frequently called Southwell equation, has been widely used by many engineers since it is simple and easy to use. Later, to obtain more accurate natural frequencies, a linear partial differential equation that governs the bending vibration of a rotating beam was derived by Schilhansl [2]. Applying Ritz method to the partial differential equation, more accurate coefficients

0022-460X/02/$35.00

for the analytical model of Southwell equation could be obtained. In the 1970s, owing to the fast progress of computing technologies, a large number of papers in which numerical methods were employed for the modal analysis of rotating structures were published. For instance, Putter and Manor [3] applied the assumed mode approximation method for the modal analysis of a rotating beam. Various other effects on the modal characteristics of rotating beams were also investigated. The effect of tip mass was considered by Hoa [4] and Wright *et al.* [5], elastic foundation and cross-section variation were considered by Kuo *et al.* [6], shear deformation was considered by Yokoyama [7] and Du *et al.* [8], and the transverse crack was considered by Wu and Huang [9]. A large number of related papers were reviewed in some survey papers (see, for instance, references [10, 11]).

Even though many rotating structures can be successfully idealized as beams some engineering structures (such as turbo-machine blades with low aspect ratios) behave like plates rather than beams. Obviously, beam models are not adequate to predicting accurate modal characteristics of plate-like structures. Therefore, the need for developing vibration models for rotating plates is clear. In spite of this need, only a few research works on the dynamics of rotating plates could be found in the literature survey conducted by the authors. Dokainish and Rawtani [12] used a finite element technique to determine the modal characteristics of rotating cantilever plates mounted on the periphery of a rotating rigid hub. A similar approach was taken by Ramamurti and Kielb [13] to determine the modal properties of twisted rotating plates. In these papers, a strain energy expression which involves the steady state in-plane stress components was used for the rotating plate. First, steady state stress components were obtained either analytically from the partial differential equations of stretching motion or numerically from the equilibrium condition between the centrifugal inertia forces and the steady state in-plane stress components. Then, the linear equations of motion were derived by using the strain energy expression in which the steady state stress components previously obtained were employed. This approach involves unnecessary assumptions and complexities which result in a two-step procedure to derive the equations of motion for rotating plates. Due to the complexities, only rough descriptions of deriving equations of motion are given in the literature.

Recently, a new linear dynamic modelling method for flexible beams undergoing overall motion was introduced (see references [14, 15]). Different from conventional linear modelling method, this linear modelling method employs a non-Cartesian deformation variable (stretch variable) to derive the equations of motion. It was proved that the use of the non-Cartesian variable led to capture accurate motion-induced stiffness variation effects. This modelling method was later successfully utilized to obtain the modal characteristics of rotating beams (see reference [16]). The accuracy and the rigorousness of the modelling method was well proved in the work. More recently, a linear dynamic modelling method was introduced by Yoo and Chung [17] for flexible plates undergoing overall motion. The dynamic modelling method for beams introduced in reference [15] is extended for plates in this paper. The key ingredient of the modelling method is the use of two in-plane stretch variables by which the exact in-plane strain energy can be expressed in a quadratic form. The use of the two stretch variables enables one to derive linear equations of motion which include proper motion-induced stiffness variation terms. The accuracy of the modelling method was examined and verified by comparing its results with some existing results. However, transient characteristics (instead of modal characteristics) of rotating plates are mostly investigated with the modelling method.

The purpose of the present paper is to investigate the modal characteristics of rotating cantilever plates. The dynamic modelling method, which was introduced in reference [17] for flexible plates undergoing overall motion, is employed to derive the equations for the modal analysis of a rotating rectangular plate. Dimensionless parameters are identified

through a dimensional analysis and the effects of the dimensionless parameters on the variations of modal characteristics are investigated. Eigenvalue loci veering and crossing phenomena, which were not previously reported in this class of problems (vibration of rotating structures), are discussed.

2. EQUATIONS OF MOTION

The system to be analyzed is a thin rectangular plate undergoing overall motion in three-dimensional space. The plate is characterized by natural length a, width b, thickness h, and material properties E (Young's modulus), G (shear modulus), ρ (mass per unit area), and v (the Poisson ratio). The Kirchhoff hypothesis for a thin plate is employed in the present work. So the transverse shear and the rotary inertia effects are ignored to simplify the formulation and to focus on the main issue of the present work, which is the variation of modal characteristics of the plate undergoing overall motion. Based on the Kirchhoff hypothesis, any straight line segments perpendicular to the mid-plane of the plate remain perpendicular to the mid-plane during deformation. Thus, any one of them can be used as a rigid reference frame for the plate. In this work, the straight line segment located at one corner of the plate is employed as a reference frame (denoted as A in Figure 1). The overall motion of the reference frame A is assumed to be prescribed in this work. The angular velocity of A and the velocity of the reference point O (shown in Figure 1), which represent the overall motion, can be expressed as

$$\boldsymbol{\omega}^A = \omega_1\hat{\boldsymbol{a}}_1 + \omega_2\hat{\boldsymbol{a}}_2 + \omega_3\hat{\boldsymbol{a}}_3, \qquad \mathbf{v}^O = v_1\hat{\boldsymbol{a}}_1 + v_2\hat{\boldsymbol{a}}_2 + v_3\hat{\boldsymbol{a}}_3, \tag{1,2}$$

where ω_i and v_i $(i = 1, 2, 3)$ are prescribed functions of time and $\hat{\boldsymbol{a}}_1$, $\hat{\boldsymbol{a}}_2$, and $\hat{\boldsymbol{a}}_3$ constitute a unit vector triad fixed to the reference frame A. As shown in Figure 2, the distances x and y are measured, respectively, along the directions of $\hat{\boldsymbol{a}}_1$ and $\hat{\boldsymbol{a}}_2$ from the reference point O to a generic point P_0 (which lies on the mid-plane of the undeformed plate). When the plate is deformed, the point P_0 moves to a new position. The displacement vector from P_0 to P (denoted by $\mathbf{u}$) can be expressed as

$$\mathbf{u} = u_1\hat{\boldsymbol{a}}_1 + u_2\hat{\boldsymbol{a}}_2 + u_3\hat{\boldsymbol{a}}_3. \tag{3}$$

The three Cartesian variables u_1–u_3 are conventionally approximated to obtain the ordinary differential equations of motion. In the present work, however, two in-plane stretch variables (s and r shown in Figure 2) along with the lateral displacement u_3 are approximated. Thus, by using the Rayleigh–Ritz method, they can be expressed as

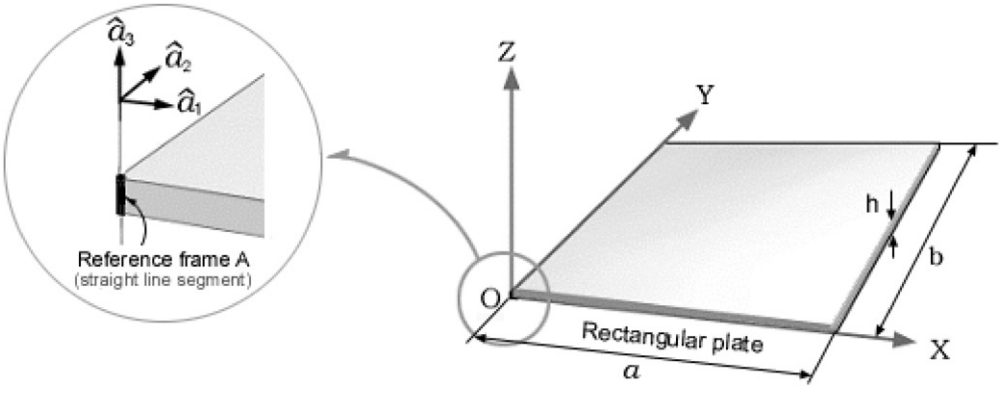

Figure 1. Configuration of a rectangular plate and its reference frame.

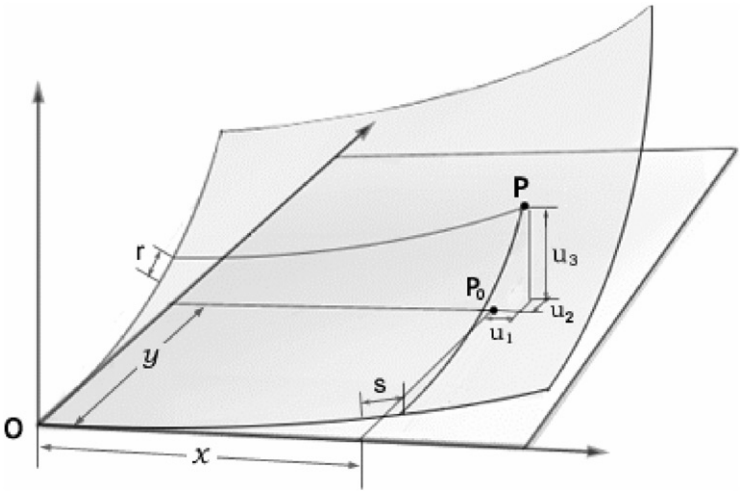

Figure 2. Deformation of the mid-plane of a plane.

follows:

$$s(x,y,t) = \sum_{j=1}^{\mu} \phi_{1j}(x,y) q_j(t), \qquad r(x,y,t) = \sum_{j=1}^{\mu} \phi_{2j}(x,y) q_j(t), \tag{4,5}$$

$$u_3(x,y,t) = \sum_{j=1}^{\mu} \phi_{3j}(x,y) q_j(t), \tag{6}$$

where ϕ_{1j}, ϕ_{2j}, and ϕ_{3j} are spatial mode functions. Any compact set of admissible functions which satisfy the geometric boundary conditions of the plate can be used as the mode functions (see reference [18]). q_j's are generalized co-ordinates and μ is the total number of the generalized co-ordinates. For the convenience of formalism, s, r, and u_3 use the same number of co-ordinates μ. However, they are not actually coupled. For instance, ϕ_{1j} is not zero only if $j \leqslant \mu_1$; ϕ_{2j} is not zero only if $\mu_1 < j \leqslant \mu_1 + \mu_2$; and ϕ_{3j} is not zero only if $\mu_1 + \mu_2 < j \leqslant \mu_1 + \mu_2 + \mu_3$. In other words, μ_1, μ_2, and μ_3 denote the actual numbers of generalized co-ordinates for s, r, and u_3 respectively. μ is the total sum of μ_1–μ_3.

The use of the two stretch variables s and r leads to the following expression of in-plane strain energy of a rectangular plate:

$$U_i = \frac{1}{2}\int_0^b \int_0^a \left[\beta_1 \left\{ \left(\frac{\partial s}{\partial x}\right)^2 + \left(\frac{\partial r}{\partial y}\right)^2 + 2\nu \left(\frac{\partial s}{\partial x}\right)\left(\frac{\partial r}{\partial y}\right) \right\} + \beta_2 \left(\frac{\partial s}{\partial y} + \frac{\partial r}{\partial x}\right)^2 \right] \mathrm{d}x\,\mathrm{d}y, \tag{7}$$

where

$$\beta_1 = \frac{Eh}{(1-\nu^2)}, \qquad \beta_2 = Gh. \tag{8,9}$$

Since the stretch variables s and r are employed in equation (7), U_i represents the exact in-plane strain energy of the plate. Now the total strain energy can be obtained as follows:

$$U = U_i + U_b, \tag{10}$$

where U_b represents the bending strain energy which is given by

$$U_b = \frac{1}{2}\int_0^b \int_0^a D\left[\left(\frac{\partial^2 u_3}{\partial x^2}\right)^2 + \left(\frac{\partial^2 u_3}{\partial y^2}\right)^2 + 2\nu\left(\frac{\partial^2 u_3}{\partial x^2}\right)\left(\frac{\partial^2 u_3}{\partial y^2}\right) + 2(1-\nu)\left(\frac{\partial^2 u_3}{\partial x \partial y}\right)^2\right] \mathrm{d}x\,\mathrm{d}y, \tag{11}$$

where

$$D = \frac{Eh^3}{12(1-\nu^2)}. \tag{12}$$

By using the total strain energy, the generalized active forces (see reference [18]) can be obtained as follows:

$$F_i = -\frac{\partial U}{\partial q_i} \quad (i = 1, 2, \ldots, \mu). \tag{13}$$

The use of s and r results in the exact in-plane strain energy which is expressed in a quadratic form. Thus, linear generalized active forces can be obtained from the strain energy. It, however, complicates the formulation of generalized inertia forces in the equations of motion. The generalized inertia forces can be obtained by using the following equation:

$$F_i^* = -\int_0^b \int_0^a \rho\left(\frac{\partial \mathbf{v}^P}{\partial \dot{\boldsymbol{q}}_i}\right) \cdot \mathbf{a}^P \,\mathrm{d}x\,\mathrm{d}y \quad (i = 1, 2, \cdots, \mu), \tag{14}$$

where $\dot{\boldsymbol{q}}_i$'s are the time derivatives of the generalized co-ordinates; and $\mathbf{v}^P$ and $\mathbf{a}^P$ are the velocity and the acceleration of the generic point P. By using the angular velocity of the reference frame A and the velocity of the reference point O, the velocity of the generic point P can be obtained as

$$\begin{aligned}\mathbf{v}^P = {} & [v_1 + \dot{\boldsymbol{u}}_1 + \omega_2 u_3 - \omega_3(y + u_2)]\hat{\boldsymbol{a}}_1 + [v_2 + \dot{\boldsymbol{u}}_2 + \omega_3(x + u_1) - \omega_1 u_3]\hat{\boldsymbol{a}}_2 \\ & + [v_3 + \dot{\boldsymbol{u}}_3 + \omega_1(y + u_2) - \omega_2(x + u_1)]\hat{\boldsymbol{a}}_3.\end{aligned} \tag{15}$$

Since u_1, u_2 and their derivatives (with respect to time) shown in equation (15) are not approximated, they need to be replaced by s, r, u_3, and their derivatives. For the replacement, the following geometric relations between the in-plane stretch variables and the Cartesian deformation variables can be utilized:

$$x + s = \int_0^x \left[\left(1 + \frac{\partial u_1}{\partial \xi}\right)^2 + \left(\frac{\partial u_3}{\partial \xi}\right)^2\right]^{1/2} \mathrm{d}\xi, \tag{16}$$

$$y + r = \int_0^y \left[\left(1 + \frac{\partial u_2}{\partial \eta}\right)^2 + \left(\frac{\partial u_3}{\partial \eta}\right)^2\right]^{1/2} \mathrm{d}\eta. \tag{17}$$

In the present work, linear equations of motion will be derived eventually. Therefore, the following approximated relations (which are obtained by using the binomial expansion of equations (16) and (17)) can be employed since the final form of equations of motion is not affected by the truncated higher degree terms.

$$s = u_1 + \frac{1}{2}\int_0^x \left[\left(\frac{\partial u_3}{\partial \xi}\right)^2\right] \mathrm{d}\xi, \qquad r = u_2 + \frac{1}{2}\int_0^y \left[\left(\frac{\partial u_3}{\partial \eta}\right)^2\right] \mathrm{d}\eta. \tag{18, 19}$$

Differentiations of equations (18) and (19) with respect to time yield

$$\dot{s} = \dot{u}_1 + \int_0^x \left[\left(\frac{\partial \dot{u}_3}{\partial \xi} \right) \left(\frac{\partial u_3}{\partial \xi} \right) \right] \mathrm{d}\xi, \quad \dot{r} = \dot{u}_2 + \int_0^y \left[\left(\frac{\partial \dot{u}_3}{\partial \eta} \right) \left(\frac{\partial u_3}{\partial \eta} \right) \right] \mathrm{d}\eta. \tag{20, 21}$$

By using equations (20) and (21) along with equations (15) and (4)–(6), the partial derivative of $\mathbf{v}^P$ with respect to $\dot{q}_i$ can be obtained as follows:

$$\frac{\partial \mathbf{v}^P}{\partial \dot{q}_i} = \left[\phi_{1i} - \sum_{j=1}^{\mu} \int_0^x \phi_{3i,\xi} \phi_{3j,\xi} d\xi q_j \right] \hat{a}_1 + \left[\phi_{2i} - \sum_{j=1}^{\mu} \int_0^y \phi_{3i,\eta} \phi_{3j,\eta} d\eta q_j \right] \hat{a}_2 + [\phi_{3i}] \hat{a}_3. \tag{22}$$

Now the acceleration of point P can be obtained by simply differentiating the velocity shown in equation (15) with respect to time. Substituting the acceleration and the partial velocities into equation (14), the generalized inertia forces can be obtained. By linearizing the generalized inertia forces and summing the generalized active forces (obtained in equation (13)), the following linear equations of motion are finally derived:

$$\begin{aligned} \sum_{j=1}^{\mu} & [M_{ij}^{11} \ddot{q}_j + (K_{ij}^{S1} + K_{ij}^{S2}) q_j + (\omega_1 \omega_2 - \dot{\omega}_3) M_{ij}^{12} q_j + (\omega_3 \omega_1 + \dot{\omega}_2) M_{ij}^{13} q_j \\ & - (\omega_2^2 + \omega_3^2) M_{ij}^{11} q_j - 2\omega_3 M_{ij}^{12} \dot{q}_j + 2\omega_2 M_{ij}^{13} \dot{q}_j] \\ & = (\omega_2^2 + \omega_3^2) X_{1i} - (\omega_1 \omega_2 - \dot{\omega}_3) Y_{1i} - (\dot{v}_1 + \omega_2 v_3 - \omega_3 v_2) Z_{1i}, \end{aligned} \tag{23}$$

$$\begin{aligned} \sum_{j=1}^{\mu} & [M_{ij}^{22} \ddot{q}_j + (K_{ij}^{S3} + K_{ij}^{S4}) q_j + (\omega_1 \omega_2 + \dot{\omega}_3) M_{ij}^{21} q_j + (\omega_3 \omega_2 - \dot{\omega}_1) M_{ij}^{23} q_j \\ & - (\omega_3^2 + \omega_1^2) M_{ij}^{22} q_j + 2\omega_3 M_{ij}^{21} \dot{q}_j - 2\omega_1 M_{ij}^{23} \dot{q}_j] \\ & = (\omega_1 \omega_2 + \dot{\omega}_3) X_{2i} + (\omega_3^2 + \omega_1^2) Y_{2i} - (\dot{v}_2 + \omega_3 v_1 - \omega_1 v_3) Z_{2i}, \end{aligned} \tag{24}$$

$$\begin{aligned} \sum_{j=1}^{\mu} & [M_{ij}^{33} \ddot{q}_j + K_{ij}^{B} q_j - (\omega_1^2 + \omega_2^2) M_{ij}^{33} q_j + (\omega_3 \omega_1 - \dot{\omega}_2) M_{ij}^{31} q_j \\ & + (\omega_3 \omega_2 + \dot{\omega}_1) M_{ij}^{32} q_j + 2\omega_1 M_{ij}^{32} \dot{q}_j - 2\omega_2 M_{ij}^{31} \dot{q}_j \\ & + (\omega_2^2 + \omega_3^2) K_{ij}^{GX2} q_j - (\dot{v}_1 + \omega_2 v_3 - \omega_3 v_2) K_{ij}^{GX1} q_j + (\omega_3^2 + \omega_1^2) K_{ij}^{GY2} q_j \\ & - (\dot{v}_2 + \omega_3 v_1 - \omega_1 v_3) K_{ij}^{GY1} q_j - (\omega_1 \omega_2 - \dot{\omega}_3) K_{ij}^{GXY} q_j] \\ & = -(\omega_3 \omega_1 - \dot{\omega}_2) X_{3i} - (\omega_2 \omega_3 + \dot{\omega}_1) Y_{3i} - (\dot{v}_3 + \omega_1 v_2 - \omega_2 v_1) Z_{3i}, \end{aligned} \tag{25}$$

where

$$M_{ij}^{ab} = \int_0^b \int_0^a \rho \phi_{ai} \phi_{bj} \, \mathrm{d}x \, \mathrm{d}y, \tag{26}$$

$$K_{ij}^{S1} = \int_0^b \int_0^a (\beta_1 \phi_{1i,x} \phi_{1j,x} + \beta_2 \phi_{1i,y} \phi_{1j,y}) \, \mathrm{d}x \, \mathrm{d}y, \tag{27}$$

$$K_{ij}^{S2} = \int_0^b \int_0^a (\beta_1 v \phi_{1i,x} \phi_{2j,y} + \beta_2 \phi_{1i,y} \phi_{2j,x}) \, \mathrm{d}x \, \mathrm{d}y, \tag{28}$$

$$K_{ij}^{S3} = \int_0^b \int_0^a (\beta_1 \phi_{2i,y} \phi_{2j,y} + \beta_2 \phi_{2i,x} \phi_{2j,x}) \, \mathrm{d}x \, \mathrm{d}y, \tag{29}$$

$$K_{ij}^{S4} = \int_0^b \int_0^a (\beta_1 \nu \phi_{2i,x} \phi_{1j,y} + \beta_2 \phi_{2i,y} \phi_{1j,x}) \, \mathrm{d}x \, \mathrm{d}y, \tag{30}$$

$$K_{ij}^{B} = \int_0^b \int_0^a D[\phi_{3i,xx} \phi_{3j,xx} + \phi_{3i,yy} \phi_{3j,yy} + \nu \phi_{3i,xx} \phi_{3j,yy} + \nu \phi_{3i,yy} \phi_{3j,xx} + 2(1-\nu) \phi_{3i,xy} \phi_{3j,xy}] \, \mathrm{d}x \, \mathrm{d}y, \tag{31}$$

$$K_{ij}^{GX2} = \int_0^b \int_0^a \frac{1}{2} \rho (a^2 - x^2) \phi_{3i,x} \phi_{3j,x} \, \mathrm{d}x \, \mathrm{d}y, \tag{32}$$

$$K_{ij}^{GX1} = \int_0^b \int_0^a \rho (a - x) \phi_{3i,x} \phi_{3j,x} \, \mathrm{d}x \, \mathrm{d}y, \tag{33}$$

$$K_{ij}^{GY2} = \int_0^b \int_0^a \frac{1}{2} \rho (b^2 - y^2) \phi_{3i,y} \phi_{3j,y} \, \mathrm{d}x \, \mathrm{d}y, \tag{34}$$

$$K_{ij}^{GY1} = \int_0^b \int_0^a \rho (b - y) \phi_{3i,y} \phi_{3j,y} \, \mathrm{d}x \, \mathrm{d}y, \tag{35}$$

$$K_{ij}^{GXY} = \int_0^b \int_0^a \rho [x(b-y) \phi_{3i,y} \phi_{3j,y} + y(a-x) \phi_{3i,x} \phi_{3j,x}] \, \mathrm{d}x \, \mathrm{d}y, \tag{36}$$

$$X_{ai} = \int_0^b \int_0^a \rho x \phi_{ai} \, \mathrm{d}x \, \mathrm{d}y, \quad Y_{ai} = \int_0^b \int_0^a \rho y \phi_{ai} \, \mathrm{d}x \, \mathrm{d}y, \quad Z_{ai} = \int_0^b \int_0^a \rho \phi_{ai} \, \mathrm{d}x \, \mathrm{d}y. \tag{37-39}$$

Equations (23)–(25) can be used for the transient analysis of a plate undergoing overall motion. Equations (23) and (24) govern the in-plane motions of the plate and equation (25) governs the lateral motion of the plate. In equation (25), several motion-induced stiffness variation terms are shown. These terms play important roles in the vibration analysis of rotating cantilever plates. In the following sections, equation (25) is particularized for a case of rotating cantilever plates and eigenanalyses are performed.

3. FORMULATION FOR VIBRATION ANALYSIS

The stretching motion is coupled with the bending motion in equations (23)–(25). The coupling effect becomes negligible for thin flexible structures (see reference [16]). Thus, the coupling effect between the stretching motion and the bending motion is assumed to be negligible in the present work. So equation (25) is used independently for the vibration analysis after ignoring all the coupling terms appearing in the equation.

Figure 3 shows a cantilever plate attached to a rigid hub A of radius R. The hub is rotating with a constant angular speed Ω. Unit vectors $\hat{\boldsymbol{a}}_1$, $\hat{\boldsymbol{a}}_2$, and $\hat{\boldsymbol{a}}_3$ fixed to the rigid hub are parallel to the direction of the length, the width, and the thickness of the undeformed plate respectively. The measure numbers of the velocity of O and the angular velocity of A in the direction of $\hat{\boldsymbol{a}}_1$, $\hat{\boldsymbol{a}}_2$, and $\hat{\boldsymbol{a}}_3$ are

$$v_1 = v_2 = 0, \qquad v_3 = -R\Omega, \qquad \omega_1 = \omega_3 = 0, \qquad \omega_2 = \Omega. \tag{40,41}$$

These measure numbers are substituted into equation (25). Ignoring the gyroscopic coupling terms (between stretching and bending) and the right-hand side terms in equation

(25), the following equation is obtained for the free vibration analysis of the rotating plate:

$$\sum_{j=1}^{\mu} [M_{ij}^{33}\ddot{q}_j - \Omega^2 M_{ij}^{33} q_j + \Omega^2 K_{ij}^{GX2} q_j + R\Omega^2 K_{ij}^{GX1} q_j + K_{ij}^{B} q_j] = 0. \tag{42}$$

It is useful to rewrite equation (42) in a non-dimensional form. For the purpose, the following non-dimensional variables are introduced:

$$\tau = \frac{t}{T}, \qquad \chi = \frac{x}{a}, \qquad \zeta = \frac{y}{b}, \qquad z_j = \frac{q_j}{a}, \tag{43–46}$$

where T is given as

$$T = \left(\frac{\rho h a^4}{D}\right)^{1/2}. \tag{47}$$

Using these dimensionless variables, a non-dimensional form of equation (42) is obtained as follows:

$$\sum_{j=1}^{\mu} [\bar{M}_{ij}\ddot{z}_j - \gamma^2 \bar{M}_{ij} z_j + \gamma^2 \bar{K}_{ij}^{GX2} z_j + \sigma\gamma^2 \bar{K}_{ij}^{GX1} z_j + \bar{K}_{ij}^{B} z_j] = 0, \tag{48}$$

where double overdots on z_j means double differentiation with respect to τ and

$$\bar{M}_{ij} = \int_0^1 \int_0^1 \psi_i \psi_j \, \mathrm{d}\chi \, \mathrm{d}\zeta, \tag{49}$$

$$\bar{K}_{ij}^{GX2} = \int_0^1 \int_0^1 \frac{1}{2}(1-\chi^2)\psi_{i,\chi}\psi_{j,\chi} \, \mathrm{d}\chi \, \mathrm{d}\zeta, \tag{50}$$

$$\bar{K}_{ij}^{GX1} = \int_0^1 \int_0^1 (1-\chi)\psi_{i,\chi}\psi_{j,\chi} \, \mathrm{d}\chi \, \mathrm{d}\zeta, \tag{51}$$

$$\begin{aligned}\bar{K}_{ij}^{B} = \int_0^1 \int_0^1 [&\psi_{i,\chi\chi}\psi_{j,\chi\chi} + \delta^4 \psi_{i,\zeta\zeta}\psi_{j,\zeta\zeta} + \nu\delta^2 \psi_{i,\chi\chi}\phi_{j,\zeta\zeta} \\ &+ \nu\delta^2 \psi_{i,\zeta\zeta}\psi_{j,\chi\chi} + 2(1-\nu)\delta^2 \psi_{i,\chi\zeta}\psi_{j,\chi\zeta}] \, \mathrm{d}\chi \, \mathrm{d}\zeta.\end{aligned} \tag{52}$$

The function ψ_i shown in equations (49)–(52), which is the function of dimensionless variables χ and ζ, has the same numerical value as the function ϕ_{3i}, which is the function of x and y. There are three parameters involved in equations (48) and (52): δ, the ratio of the plate width to its length (the aspect ratio); σ, the ratio of the rigid hub radius to the plate

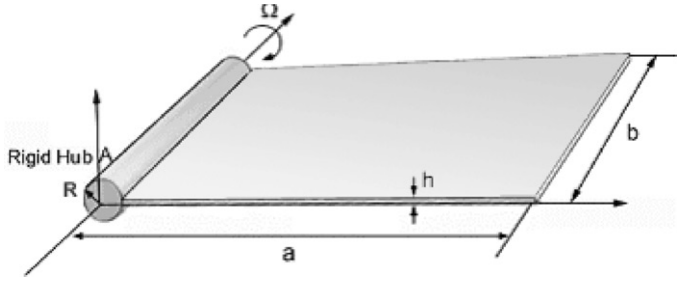

Figure 3. Configuration of a rotating cantilever plate.

length; and γ, the dimensionless angular speed. These parameters are given as follows:

$$\delta = \frac{a}{b}, \qquad \sigma = \frac{R}{a}, \qquad \gamma = \Omega T. \tag{53-55}$$

From the non-dimensional equation (48), the free vibration eigenvalue problem of a rotating cantilever plate can be obtained by assuming that the z_i's are harmonic functions of τ (dimensionless time). Defining a column matrix $\mathbf{z}$ whose elements are the z_i's, one has

$$\mathbf{z} = \mathrm{e}^{\mathrm{j}\omega\tau}\mathbf{Z}, \tag{56}$$

where ω is the dimensionless natural frequency which can be obtained by multiplying the natural frequency of the rotating plate by T, and $\mathbf{Z}$ is a constant vector characterizing the deflection shape for synchronous motion. Substituting equation (56) into equation (48) yields the following discrete eigenvalue problem:

$$\omega^2\mathbf{M}\mathbf{Z} = \mathbf{K}\mathbf{Z}, \tag{57}$$

where $\mathbf{M}$ and $\mathbf{K}$ are square matrices whose respective elements M_{ij} and K_{ij} are given by

$$M_{ij} = \bar{M}_{ij}, \qquad K_{ij} = \bar{K}^B_{ij} z_j - \gamma^2 \bar{M}_{ij} + \gamma^2 \bar{K}^{GX2}_{ij} + \sigma\gamma^2 \bar{K}^{GX1}_{ij}. \tag{58, 59}$$

4. NUMERICAL RESULTS

To solve the eigenvalue problem formulated in equation (57) for the rotating plate, assumed mode functions are needed. In the present work, five cantilever beam mode functions and seven free–free beam mode functions which include two rigid body mode functions are combined (see reference [19]) to generate 35 plate mode functions. To check the convergence of the lowest five natural frequencies, results for the three cases of employing mode functions are given in Table 1. Fifteen mode functions are employed for the first case, 35 mode functions are employed for the second case, and 63 mode functions are employed for the third case. The maximal difference between the second and the third results is less than 0·2%, which indicates the sufficient convergence. Therefore, 35 mode functions are employed to obtain all the results in this study.

In this study, the coupling effects between the stretching and the bending equations are assumed to be negligible. To check the validity of the assumption, numerical results considering the coupling terms are obtained. A typical set of parameters is employed to obtain the results. In Table 2, the results are compared with those obtained by not considering the coupling terms. The maximal difference is less than 2% even though the non-dimensional angular speed γ is 10 and the slenderness ratio is 20. As mentioned earlier, the coupling effects only become important for quite large non-dimensional angular speed and small slenderness ratio. Therefore, the coupling effects, even though it can be considered if needed, will be ignored in this study.

To prove the reliability of the modelling method presented in this paper, the results obtained by using the present modelling method are compared to the results obtained by using the existing method (see reference [12]). The parameters used to obtain the results are shown in Tables 3 and 4. As shown in the tables, the results obtained by the present modelling method are in reasonable agreement with the results obtained by the existing method.

Figure 4 shows the variations of the lowest five dimensionless natural frequencies of rotating square plates ($\delta = 1$). The solid lines in the figures are for zero hub radius ratio ($\sigma = 0$), while the dotted lines are for $\sigma = 1$. As expected intuitively, the dimensionless natural frequencies increase as the angular speed ratio increases. The increasing rates

TABLE 1

Convergence of lowest five natural frequencies for the three cases of employing mode functions ($\delta = 1,\ \sigma = 1$)

Non-dimensional angular speed	Mode	Case 1		Case 2		Case 3	
		x 3	y 5	x 5	y 7	x 7	y 9
$\gamma = 10$	1	13·332		13·273		13·260	
	2	15·426		15·311		15·288	
	3	30·000		29·792		29·734	
	4	43·579		43·289		43·230	
	5	49·103		48·851		48·768	

TABLE 2

Comparison of lowest five natural frequencies with and without the coupling effect ($\delta = 1,\ \gamma = 10,\ \alpha = 20$)

Hub ratio	Mode	Results with no coupling	Results with coupling
$\sigma = 0$	1	5·0491	4·9679
	2	9·0322	8·9289
	3	26·761	26·761
	4	32·350	32·347
	5	39·078	39·068
$\sigma = 1$	1	13·273	13·056
	2	15·311	15·130
	3	29·792	29·792
	4	43·289	43·286
	5	48·851	48·838

(slopes of trajectories) become larger as the hub radius ratio σ increases. These result from the centrifugal inertia force which increases as the angular speed or the hub radius increases.

An interesting phenomenon can be observed from Figure 4. The third and fourth eigenvalue loci approach each other as the angular speed increases; however, they do not cross, but veer away from each other. This phenomenon is referred to as eigenvalue loci veering. Eigenvalue loci veering was first discussed in engineering systems by Leissa [20]. Later, similar veering phenomena were also observed in other engineering examples (see references [21, 22]). In these examples in references [20–22], however, eigenvalue loci converge toward each other very closely before veering away. Compared to the abrupt loci veerings, those displayed in Figure 4 for the rotating cantilever plate are mild: the eigenvalue loci, although clearly veering, are always substantially separated from each other. Considering that the number of modal functions used in the present analysis is sufficient to insure adequate convergence for the lowest five eigensolutions, it is clear that the loci veering in Figure 4 do not result from numerical approximation. Indeed, the minimum distance between the third and the fourth loci in Figure 4 did not decrease when more assumed mode functions were employed, thereby preserving the veering.

The diminishing distance between particular eigenvalues as the angular speed increases can be explained by examining the associated mode shapes. Since the cantilever plate is

TABLE 3

Comparison of lowest five natural frequencies by the present and Southwell methods ($\delta = 1,\ \sigma = 0$)

Non-dimensional angular speed	Mode	Present method	Southwell method
$\gamma = 1$	1	3·5156	3·5136
	2	8·5328	8·5282
	3	21·520	21·525
	4	27·353	27·402
	5	31·206	31·458
$\gamma = 2$	1	3·5963	3·5791
	2	8·5507	8·5324
	3	21·865	21·894
	4	27·384	27·691
	5	31·477	32·113

TABLE 4

Comparison of lowest five natural frequencies by the present and Southwell methods ($\delta = 1,\ \sigma = 1$)

Non-dimensional angular speed	Mode	Present method	Southwell method
$\gamma = 1$	1	3·7324	3·7299
	2	8·6240	8·6138
	3	21·706	21·710
	4	27·394	27·554
	5	31·350	31·760
$\gamma = 2$	1	4·3805	4·3676
	2	8·9087	8·8699
	3	22·580	22·612
	4	27·557	28·288
	5	32·043	33·620

rotating about an axis (which is parallel to the vertical direction of the plate), the eigenvalue corresponding to the mode shape with vertical nodal lines increases faster than that with horizontal nodal lines. This is because the rotation has a greater effect on the bending modes. For example, the third and fourth modes have primarily vertical and horizontal nodal lines for zero speed, as shown in Figure 5. This discussion explains why two particular eigenvalue loci converge toward each other as γ increases. Thus, it seems that the two loci should cross each other eventually. However, as shown in Figure 4, they veer away rather than cross. Then how could they avoid crossing? The answer to this question can be found by observing the mode shapes of the two eigenvalue loci.

Figure 6 displays the lowest five nodal line patterns for the rotating square cantilever plate. The hub radius ratio σ is equal to 0 and the non-dimensional rotating speed γ is equal to 10. Comparing these mode shapes to those of the non-rotating plate shown in Figure 5, the third and the fourth modes seem to switch their shapes (with their nodal lines having opposite concavities). Clearly from Figure 4, this mode switching is associated with

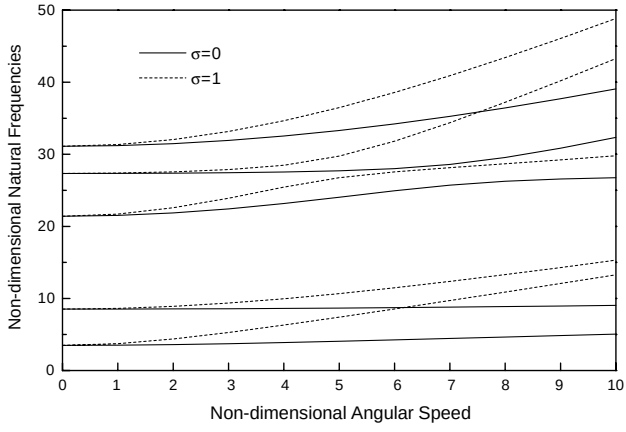

Figure 4. Lowest five natural frequencies versus angular speed for rotating square cantilever plate ($\delta = 1$).

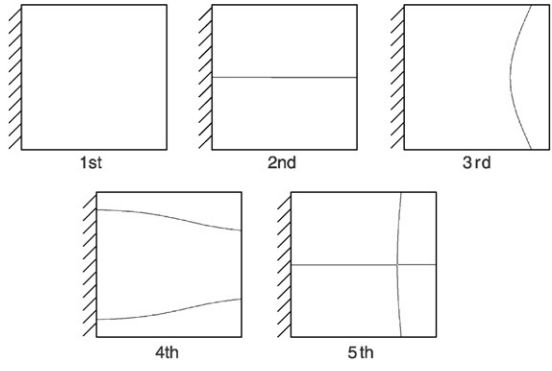

Figure 5. Nodal lines of the lowest five mode shapes on non-rotating square cantilever plates.

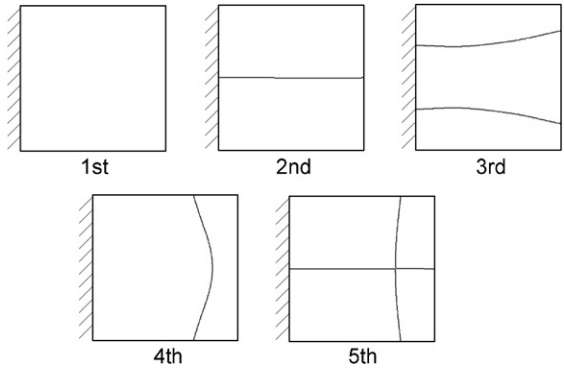

Figure 6. Nodal lines of the lowest five mode shapes of rotating square cantilever plates ($\sigma = 0,\ \gamma = 10$).

the mild veering (between the third and the fourth loci) which occurs continuously. Thus, the changes of the mode shapes should be also continuous. To verify this speculation, the nodal line patterns of the third and the fourth loci for various angular speeds are displayed in Figures 7 and 8. Initially, the third mode has primarily vertical nodal lines while the

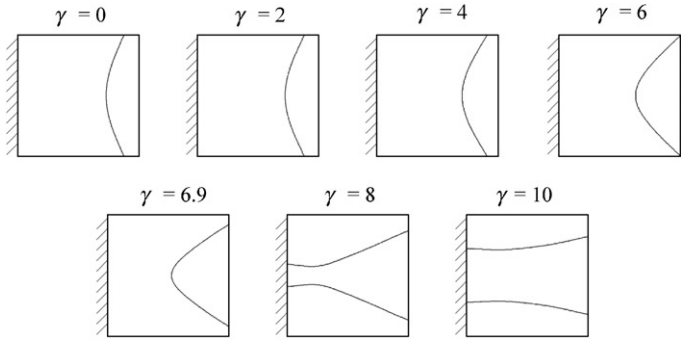

Figure 7. Variation of the third mode shape nodal lines versus angular speed change ($\sigma = 0$).

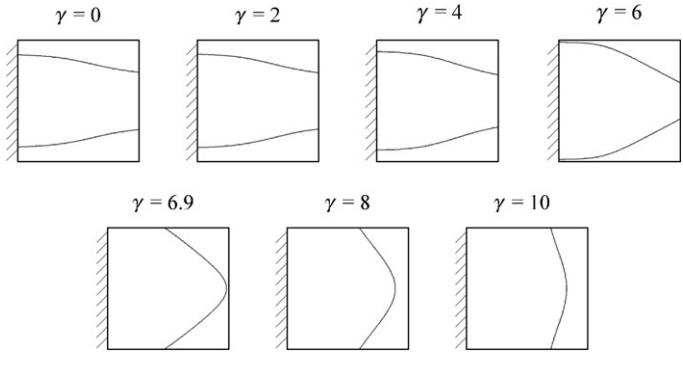

Figure 8. Variation of the fourth mode shape nodal lines versus angular speed change ($\sigma = 0$).

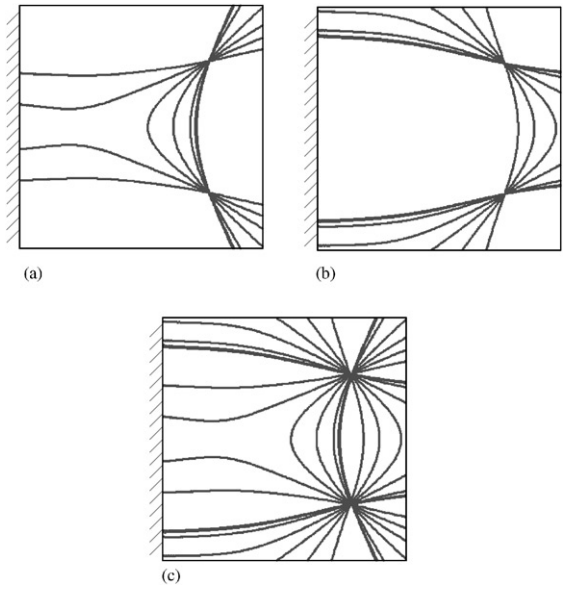

Figure 9. Superposition of the nodal lines of the third and the fourth mode shapes.

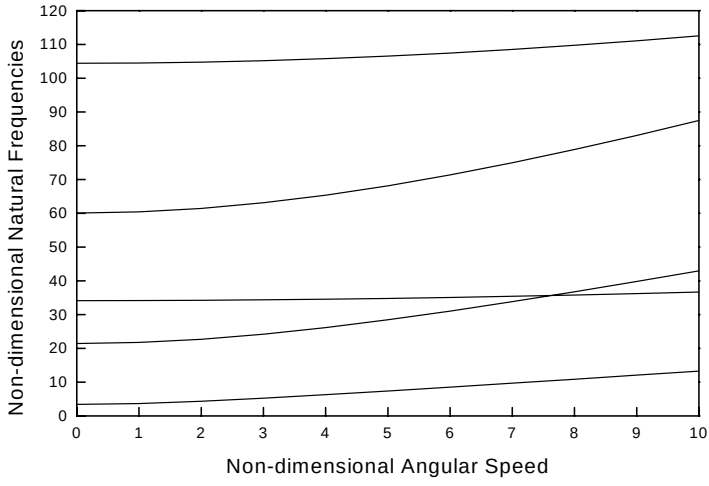

Figure 10. Lowest five natural frequencies versus angular speed for rotating rectangular cantilever plate ($\delta = 5,\ \sigma = 1$).

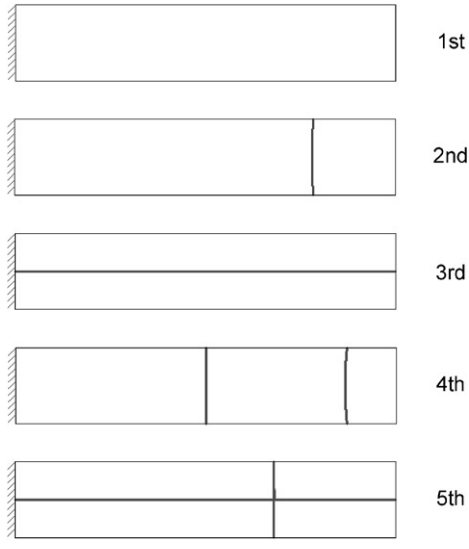

Figure 11. Nodal lines of the lowest five mode shapes for non-rotating rectangular cantilever plate ($\delta = 5,\ \sigma = 1$).

fourth mode has horizontal ones. As the dimensionless angular speed increases (and the two loci approach each other), the nodal lines become more and more "bi-directional". At the angular speed where the two eigenvalues are closest, the two mode shapes become very similar and their nodal lines are slanted at 45°. As the angular speed increases more and leaves the veering region, the modes return to the one-directional nodal line pattern except that their position has changed. Since the fourth mode has the vertical nodal lines (which characterize the third mode before the veering) after the veering, the fourth eigenvalue locus increases faster than the third eigenvalue locus. Incidentally, it is also worth noting that the concavity of the nodal lines of both mode shapes shown in Figure 7 changes during the veering. Figure 9 shows the superpositions of nodal lines obtained in

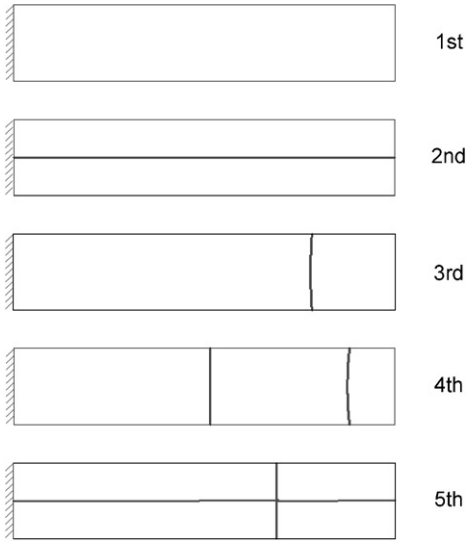

Figure 12. Nodal lines of the lowest five mode shapes for rotating rectangular cantilever plate ($\delta = 5$, $\sigma = 1$, $\gamma = 10$).

Figures 7 and 8. Observe that two points of the plate are common to all nodal lines of the third and the fourth mode shapes. Figure 9 also exhibits that the families of nodal lines for the two mode shapes possess the same two common points.

The effect of the aspect ratio on the variations of the natural frequencies is shown in Figure 10. The variations of the lowest five dimensionless natural frequencies of rotating rectangular plates with aspect ratio $\delta = 5$ and hub radius ratio $\sigma = 1$ are shown in the figure. It can be found from Figure 10 that the second and the third loci cross each other. Figures 11 and 12, respectively, show the five mode shapes when the plate is stationary and rotating (with $\gamma = 10$). One can clearly observe that the second and the third mode shapes switch their position. It can be also found that the crossing occurs between symmetric and skew-symmetric modes.

5. CONCLUSIONS

A simple and consistent formulation for deriving the linear equations of motion governing the free vibration of rotating cantilever rectangular plates is presented. The formulation eliminates unnecessary, complicated, and perhaps inconsistent steps involved in other previous methods and provides an accurate modelling for the vibration analysis of rotating plates. It is shown that the rotating plate's natural frequencies increase with both the angular speed and the hub radius. Some natural frequencies increase faster than others with the angular speed, resulting in the phenomena of eigenvalue loci veering and crossing. When two loci cross, the corresponding mode shapes remain nearly unchanged and simply change position. When two loci veer, drastic mode shape variations occur continuously in the veering region. It is found that the concavities of the nodal lines are reversed and there exist two nodal points which are common to all nodal lines of the two veering loci. For the problem presented in this paper, eigenvalue loci veering occurs between two symmetric modes while eigenvalue crossing occurs between symmetric and skew-symmetric modes.

ACKNOWLEDGMENTS

This research was supported by Center of Innovative Design Optimization Technology (iDOT), Korea Science and Engineering Foundation.

REFERENCES

1. R. Southwell and F. Gough 1921 *British A.R.C. Reports and Memoranda* No. 766. The free transverse vibration of airscrew blades.
2. M. Schilhansl 1958 *Journal of Applied Mechanics Transactions of American Society of Mechanical Engineers* **25**, 28–30. Bending frequency of a rotating cantilever beam.
3. S. Putter and H. Manor 1978 *Journal of Sound and Vibration* **56**, 175–185. Natural frequencies of radial rotating beams.
4. S. Hoa 1979 *Journal of Sound and Vibration* **67**, 369–381. Vibration of a rotating beam with tip mass.
5. A. Wright, C. Smith, R. Thresher and J. Wang 1982 *Journal of Applied Mechanics* **49**, 197–202. Vibration modes of centrifugally stiffened beams.
6. Y. Kuo, T. Wu and S. Lee 1994 *Computers and Structures* **22**, 229–236. Bending vibration of a rotating non-uniform beam with tip mass and an elastically restrained root.
7. T. Yokoyama 1988 *International Journal of Mechanical Science* **30**, 743–755. Free vibration characteristics of rotating Timoshenko beams.
8. H. Du, M. Lim and K. Liew 1994 *Journal of Sound and Vibration* **175**, 505–523. Power series solution for vibration of a rotating Timoshenko beam.
9. M. Wu and S. Huang 1998 *Shock and Vibration* **5**, 317–323. On the vibration of a cracked rotating blade.
10. A. Leissa 1981 *Applied Mechanics Reviews* **34**, 629–635. Vibration aspects of rotating turbomachinery blades.
11. J. Rao 1987 *Shock Vibration Digest* **19**, 3–10. Turbomachine blade vibration.
12. M. Dokainish and S. Rawtani 1971 *International Journal for Numerical Methods in Engineering* **3**, 233–248. Vibration analysis of rotating cantilever plates.
13. V. Ramamurti and R. Kielb 1984 *Journal of Sound and Vibration* **97**, 429–449. Natural frequencies of twisted rotating plates.
14. T. Kane, R. Ryan and A. Banerjee 1987 *Journal of Guidance, Control, and Dynamics* **10**, 139–151. Dynamics of a cantilever beam attached to a moving base.
15. H. Yoo, R. Ryan and R. Scott 1995 *Journal of Sound and Vibration* **181**, 261–278. Dynamics of flexible beams undergoing overall motions.
16. H. Yoo and S. Shin 1998 *Journal of Sound and Vibration* **212**, 807–828. Vibration analysis of rotating cantilever beams.
17. H. Yoo and J. Chung 2001 *Journal of Sound and Vibration* **239**, 123–137. Dynamics of rectangular plates undergoing prescribed overall motions.
18. T. Kane and D. Levinson 1985 *Dynamics*: *Theory and Applications*. New York: McGraw-Hill Book Company.
19. A. Leissa 1969 *NASA SP* 160. Vibration of plates.
20. A. Leissa 1974 *Journal of Applied Mathematics and Physics* **25**, 99–111. On a curve veering aberration.
21. J. Kuttler and V. Sigillito 1981 *Journal of Sound and Vibration* **75**, 585–588. On curve veering.
22. N. Perkins and C. Mote 1986 *Journal of Sound and Vibration* **106**, 451–463. Comment on curve veering in eigenvalue problems.